

# Laser-Induced Backside Wet Etching of SiO<sub>2</sub> with a Visible Ultrashort Laser Pulse by Using KMnO<sub>4</sub> Solution as an Absorber Liquid

M. Ehrhardt\*, P. Lorenz\*\*, B. Han\*, R. Zhu\*, K. Zimmer\*\*

\* *Laser-Material Interaction Lab, 2011 Co-innovation Center, Nanjing University of Science & Technology, 210094 Nanjing, People's Republic of China*

*E-mail: hanbing@njust.edu.cn*

\*\* *Leibniz Institute of Surface Modification, Permoserstr. 15, 04318 Leipzig, Germany*

Laser-induced backside wet etching (LIBWE) is a method for the precise etching and structuring of SiO<sub>2</sub>. In this study, LIBWE is performed by using ultrashort laser pulses with a pulse duration of  $\tau = 500$  fs and a wavelength of  $\lambda = 515$  nm. Saturated aqueous KMnO<sub>4</sub> solution is the absorbing liquid for the LIBWE process. The observed etching rate is approximately  $10^{-3}$  nm/pulse, which is substantially lower than that in previous reports; it increases with increasing laser fluence. The initial etching rate decreases with higher pulse numbers until it approaches a stable value. After the LIBWE, the generated etching pits are partially covered by MnO<sub>x</sub> layers with thicknesses of tens of nanometers. However, at the etched SiO<sub>2</sub> surface, two different laser-induced periodic surface structures (LIPSS) are found. In the center of the etching pits, LIPSS with a period of  $\lambda_{\text{HSFL}} \approx (52 \pm 2)$  nm are observed, whereas in the outer areas, LIPSS with a period of  $\lambda_{\text{LSFL}} \approx (390 \pm 20)$  nm are found. The etching mechanism for the LIBWE of SiO<sub>2</sub> with aqueous KMnO<sub>4</sub> solution is proposed to comprise laser-based heating, decomposition of KMnO<sub>4</sub>, and chemical etching of the SiO<sub>2</sub> surface by the produced KOH.

DOI: 10.2961/jlmn.2018.02.0001

**Keywords:** LIBWE, KMnO<sub>4</sub>, LIPSS, femtosecond, SiO<sub>2</sub>

## 1. Introduction

Laser-induced backside wet etching (LIBWE) is a method for the precise etching and structuring of transparent materials, such as fused silica, sapphire, MgF<sub>2</sub>, and poly(methyl methacrylate) (PMMA). The material etching process with LIBWE is characterized by a low etching rate and a high surface quality. With LIBWE, the rear side of a transparent sample is in contact with an absorbing liquid to allow laser photon absorption. The applied laser pulses pass through the transparent sample and are absorbed in the liquid near the interface with the sample surface. The deposited laser energy induces manifold processes including rapid heating of the surface/liquid near-interface region, surface melting/softening, bubble generation, plasma formation, and surface modification. Finally, these effects cause etching of the sample surface. Various dye/organic-solvent combinations, such as pyrene/toluene [1], pyrene/acetone [2, 3], and naphthalene/methyl methacrylate [2], as well as pure toluene [3, 4], have been reported to be applied as absorbing liquids for LIBWE using UV laser pulses. For LIBWE using visible- (VIS-) and near-infrared- (NIR-) wavelength laser pulses, absorbers such as gallium [5, 6], mercury [7], rose bengal/acetone [8], and inorganic metal salts have been tested. In the case of inorganic salts, the use of an aqueous CuSO<sub>4</sub> solution in combination with an NIR laser has attracted increasing attention in recent years [9-12]. In the pioneering work of Shafeev and co-

workers [13, 14], inorganic solutions of CrO<sub>3</sub>, FeCl<sub>3</sub>, and KMnO<sub>4</sub> were introduced for metallization and etching of sapphire by using a copper vapor laser with a wavelength of  $\lambda = 510$  nm.

LIBWE experiments are mainly performed with nanosecond laser pulses. Only a few papers cover LIBWE using ultrashort laser pulses. However, LIBWE etching with laser pulse durations in the pico- and femtosecond range is of fundamental interest: on the one hand for investigation of the LIBWE process itself, and on the other hand as a model system for studying laser-irradiation effects, either at modified surfaces or under confinement conditions. With pulse durations of less than 10 ps, thermal-dominated etching effects, which are discussed with nanosecond LIBWE, are reduced and non-linear effects have to be considered as well, because of the high photon intensity in the pico- and femtosecond time range and the short heat-diffusion length. Due to the short pulse duration and high photon density relative to those with nanosecond laser pulses, new interaction processes between the absorber liquid/sample material and the laser photon have to be considered. Such extra non-linear processes may include multiphoton absorption and non-thermal laser-induced defect generation and accumulation [15].

Böhme et al. [15, 16] investigated a pyrene/toluene solution as the absorber liquid for LIBWE with ultraviolet (UV) and NIR ultrashort laser pulses. The femtosecond LIBWE mechanism with the dye/organic solvent was explained by Böhme et al. [17] as a two-step process. In the

first step, the excited pyrene/toluene absorber solution promotes the modification of the sample surface as a result of the formation of a thin defect-enriched near-surface layer. The surface modification increases the absorption and, in consequence, the interaction of laser photons with the sample surface, which finally causes material removal. In refs. [18, 19], picosecond LIBWE of SiO<sub>2</sub>, sapphire, and fluorides by using UV laser pulses and a pyrene/toluene absorber solution has been reported. It was also speculated in that investigation that surface modification and the laser pulse – surface modification interaction are the main factors of the etching process.

In ref. [20], a comparison between various nanosecond and ultrashort laser pulse sources was performed for metallization and LIBWE with aqueous CuSO<sub>4</sub>-based absorber liquids. In contrast to the nanosecond laser pulse sources, no LIBWE or controlled metallization could be achieved with ultrashort laser pulses. Ripples or laser-induced periodic surface structures (LIPSS) have been observed for LIBWE processing with organic absorber liquids in combination with sub-picosecond and femtosecond laser pulses [15, 21]. LIPSS formation is regularly observed after processing of the surface with ultrashort laser pulses [22–24]. Two different types of LIPSS can be distinguished: low spatial frequency LIPSS (LSFL) and high spatial frequency LIPSS (HSFL). The LSFL typically have a period between  $\lambda_{LSFL} \approx \lambda$  and  $\lambda_{LSFL} \approx \lambda/n$ , with  $\lambda$  being the laser wavelength and  $n$  being the refraction index. The formation of LSFL is commonly related with effects like excitation of surface plasmon polaritons (SPP) or radiation remnants (RR) [25]. HSFL have a period less than half of the laser wavelength and are preferentially formed close to the damage threshold of the laser-irradiated surface [25]. The origin of HSFL is still under discussion, and various explanations for HSFL formation can be found in the literature [26–29]. In several studies, it could be shown that the periods of LIPSS generated in liquid environments by using ultrashort laser pulses are significantly smaller than those of LIPSS formed in air [30]. In ref. [21], LIPSS formation by LIBWE etching of SiO<sub>2</sub> with toluene as the absorber and a laser pulse duration of 600 fs was reported. The laser wavelength in this study was 248 nm. The observed LIPSS had a period of 140 nm, which is close to the laser wavelength with consideration of the refraction index of SiO<sub>2</sub>. However, only this one type of LIPSS was found; with higher fluences, the LIPSS vanished and the surface became smooth. This effect could be explained by thermal diffusion effects, which wash out the shallow nano-sized HSFL [25].

In the present study, LIBWE processing of SiO<sub>2</sub> by using VIS laser pulses with sub-picosecond durations ( $\tau = 500$  fs) and a saturated aqueous KMnO<sub>4</sub> solution has been investigated in order to study the etching of SiO<sub>2</sub> and LIPSS formation under confinement with a non-organic absorber liquid. The large absorption of the saturated aqueous KMnO<sub>4</sub> solution at the laser wavelength of  $\lambda = 515$  nm [31] is related to the manganate, whereas the water has a negligible absorption. The usage of an aqueous KMnO<sub>4</sub> solution introduces an additional absorber liquid for LIBWE with ultrashort laser pulses. The large absorption of the aqueous KMnO<sub>4</sub> solution in contrast to that of pure water enables the study of confined ablation and LIPSS formation by near-interface absorption in comparison to the non-

linear absorption with pure water. The large linear absorption of the KMnO<sub>4</sub> solution, however, reduces the required laser pulse energy to a level at which subtle laser–material interactions can be observed and not eliminated by the subsequent thermal processes in the excited system.

The influence of the laser pulse energy, the pulse number, and the pulse repetition rate on the etching rate of SiO<sub>2</sub> was investigated. The results are discussed in detail, and an etching mechanism for LIBWE with an aqueous KMnO<sub>4</sub> solution is proposed. The LIBWE-processed surface was analyzed by scanning electron microscopy (SEM) and white-light interference microscopy (WLIM).

## 2. Experimental details

A detailed description of the basic experimental setup for LIBWE can be found in refs. [32, 33]. In Figure 1, a sketch is shown of the setup for the performed experiments.

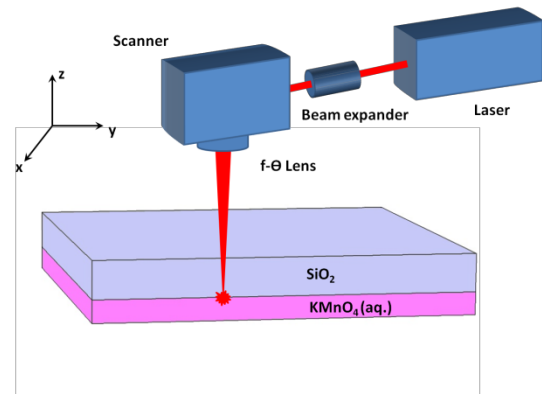
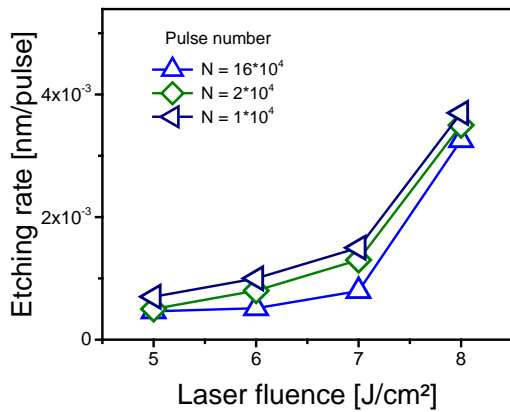


Fig.1 Sketch of the experimental setup for LIBWE.

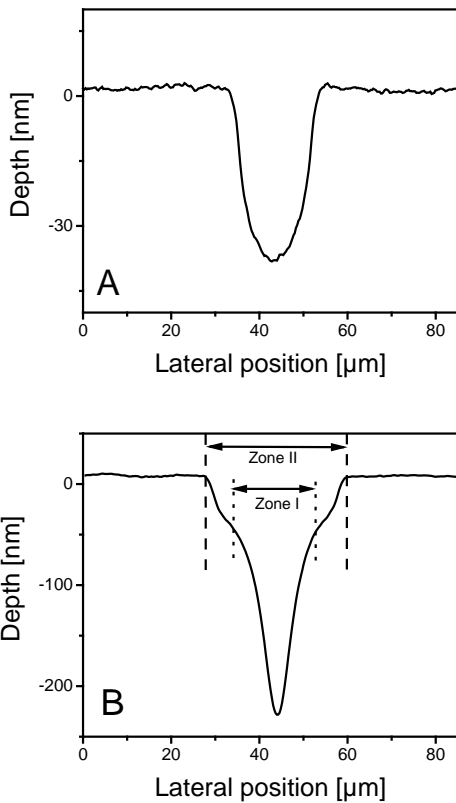
In this study, a femtosecond laser (JenLas® femto 16, Jenoptik AG, Jena, Germany) delivered laser pulses with a pulse length of  $\tau = 500$  fs at a wavelength of  $\lambda = 1030$  nm/ $\lambda = 515$  nm and a maximum repetition rate of  $f_{rep} = 500$  kHz. The output beam of the laser was linearly polarized. For the experiments, a wavelength of  $\lambda = 515$  nm with a maximum pulse energy of  $E = 109$   $\mu$ J was selected. The laser beam spot was moved across the sample by using a scanner with a telecentric  $f-\theta$  lens that had a focal length of  $f = 100$  mm. The spot size of the laser beam in the focal plane was  $d \approx 35$   $\mu$ m. For all experiments, double-sided polished fused silica pieces with a thickness of 380  $\mu$ m, surface roughness of 0.25 nm rms, and peak-to-valley value of 1.2 nm were used. The samples were used as received without further cleaning. A saturated aqueous KMnO<sub>4</sub> solution was used as the absorber liquid. After laser processing, the samples were cleaned with acidic sulfur in an ultrasonic bath for 5 min. The surface morphology and chemical composition of the laser-irradiated samples were analyzed by SEM and energy-dispersive X-ray spectroscopy (EDX), respectively. The depths of the achieved etching pits were measured by WLIM. The etching rate was calculated by dividing the measured maximum final etching depth  $d_{etch}$  by the pulse number  $N$  and, therefore, corresponds to an averaged etching rate.

3. Results



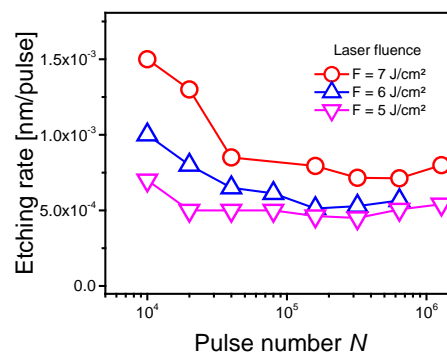
**Fig.2** Dependence of the average etching rate on the fluence used for different pulse numbers  $N$ . The lines are for guiding the eyes.

In Figure 2, the etching rate dependence on the fluence used for different pulse numbers is shown. It can be seen in Figure 2 that the etching rate increases with increasing fluence. The etching rate increase is non-linear with the fluence and features a steeper slope at higher fluences. The calculated average etching rate values are approximately  $10^{-3}$  nm/pulse, which is less than the etching of one monolayer of  $\text{SiO}_2$  per laser pulse.



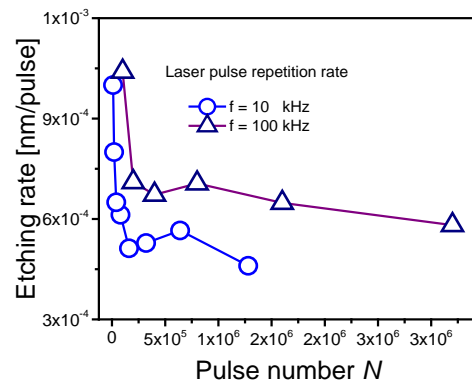
**Fig.3** Profiles from WLIM measurements of two different etching pits realized at laser fluences of  $F = 5 \text{ J/cm}^2$  (A) and  $F = 8 \text{ J/cm}^2$  (B). Both etching pits were generated by applying  $N = 80 \times 10^3$  laser pulses at  $f_{\text{rep}} = 10 \text{ kHz}$ .

Figure 3 shows the profiles of typical etching pits generated at low (A) and high (B) fluences. A comparison of the different etching pit profiles shows that the etching pits that were generated at higher fluences feature a step in the etching profile. This step allows two areas to be distinguished in the etching pit. In Figure 3 (B), these areas are marked as zone I and zone II; the laser energy density in the outer zone II was lower than that in the center zone I because of the Gaussian beam profile of the laser source used. The division of the etching pit profiles into two zones is more obvious at higher fluences. At low laser fluences, no separation of the etching pit profile can be made, as illustrated in Figure 3 (A). In Figure 4, the dependence of the etching rate on the pulse number is shown for different fluences. It can be seen that the etching rate decreases with increasing pulse numbers for  $N < 40 \times 10^3$ . In contrast, for pulse numbers higher than this, the etching rate is nearly independent from the pulse number.



**Fig.4** Etching rate dependence on the pulse number for different fluences. The lines are for guiding the eyes

A comparison of the etching rate dependences on the pulse number  $N$  shows that the etching rate achieved at  $f_{\text{rep}} = 100 \text{ kHz}$  is higher than that at  $f_{\text{rep}} = 10 \text{ kHz}$  (Figure 5). The slope of the etching rate dependence on the pulse number is similar for both pulse repetition values. The different repetition rates do not affect the primary laser-material interaction but do have an impact on subsequent processes, such as the heat accumulation of laser pulse trains and bubble formation.



**Fig.5** Etching rate dependence on the pulse number for two pulse repetition rates at  $F = 6 \text{ J/cm}^2$ . The lines are for guiding the eyes.

The SEM images in Figure 6 show an etching pit after LIBWE processing and without further cleaning. A material layer was clearly deposited in the etching pit; the deposited material layer is higher than the surrounding unprocessed substrate surface at the edge of the etching pit. An EDX spectrum measured at the center of the pit shows that the deposited layer consists mainly of  $MnO_x$ , which can be generated by decomposition of the  $KMnO_4$  absorber liquid as a result of laser irradiation.

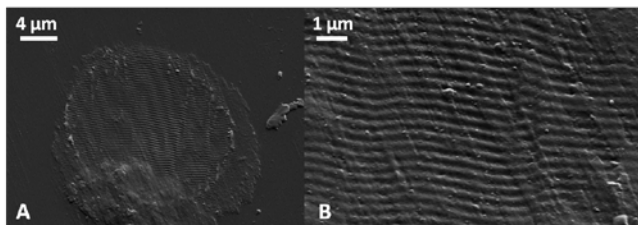


**Fig.6** (A) SEM image of an etching pit without further cleaning. (B) Magnified view of the center of the etching pit shown in (A). Conditions:  $F = 5 \text{ J/cm}^2$ ;  $N = 4 \times 10^3$ .

The thickness of the  $MnO_x$  layer was determined by measuring the depth of the etching pit before removal of the  $MnO_x$  layer and after cleaning of the sample surface. In Figure 7 (A), the dependence of the  $MnO_x$  layer thickness on the pulse number  $N$  is shown. The corresponding etching rate is also shown in this graph. It can be seen that, the  $MnO_x$  layer thickness increases with increasing pulse numbers at  $N < 40 \times 10^3$ , whereas it slightly decreases at larger pulse numbers. The dependence of the etching rate development on the pulse number  $N$  shows the opposite characteristic. This means that a higher etching rate can be achieved with a smaller  $MnO_x$  layer thickness. The same characteristic was also found for larger pulse repetition rates and pulse numbers, as can be seen in Figure 7 (B). At small pulse numbers, the  $MnO_x$  layer thickness is greater than the depth of the etching pit; in consequence, the laser-processed area is raised above the surrounding substrate surface.

The SEM image in Figure 6 (B) shows a magnified image of the center of the etching pit shown in Figure 6 (A). LIPSS with a period of  $322 \pm 30 \text{ nm}$  clearly appear on the  $MnO_x$  layer that is formed during the etching process at  $F = 5 \text{ J/cm}^2$ . In Figure 8 (A), the etching pit is shown after removal of the  $MnO_x$  layer. The LIPSS also appear on the etched  $SiO_2$  substrate but with a slightly larger period of  $390 \pm 20 \text{ nm}$ . It can be concluded that LIPSS generation is not limited to the  $MnO_x$  layer but is a principal characteristic of the etching under the applied conditions.

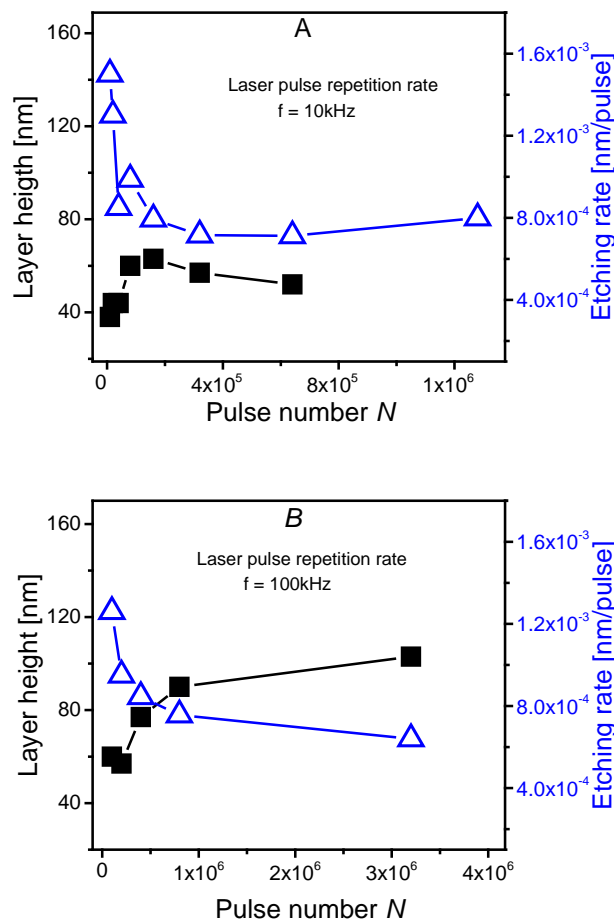


**Fig.7** Dependence of the thickness of the deposited layer (black, solid squares) and the corresponding etching rate (blue, empty triangles) on the pulse number. Conditions: (A)  $f_{\text{rep}} = 10 \text{ kHz}$ ; (B)  $f_{\text{rep}} = 100 \text{ kHz}$ .

Figure 8 (C) shows a magnified section of the LIPSS on the  $SiO_2$  substrate shown in Figure 8 (B). In addition to the LSFL, HSFL are formed inside the LSFL. The orientation of the HSFL is perpendicular to that of the LSFL. The period of these HSFL is  $\lambda_{\text{HSFL}} = 46 \pm 13 \text{ nm}$ , which is much smaller than that of the LSFL ( $\lambda_{\text{LSFL}} = 390 \pm 20 \text{ nm}$ ) and the laser wavelength ( $\lambda = 515 \text{ nm}$ ).

At higher fluence ( $F = 8 \text{ J/cm}^2$ ), the morphology of the etching pit, shown in Figure 8 (D), is different than that achieved at lower fluences (see Figure 8 (A)). However, LIPSS formation has also been observed under these conditions, as shown in Figure 8 (D) and (E). In the center of the etching pit, no LSFL can be found, and, in consequence, the surface roughness in the center is lower than at the edges of the etching pit. The magnified view of the center of the etching pit (Figure 8 (E) and (F)) shows that it is covered with HSFL, and the LSFL are at the edges. The period of the HSFL is  $\lambda_{\text{HSFL}} = 52 \pm 2 \text{ nm}$ . The period and orientation of these HSFL are similar to those of the HSFL inside the LSFL at low energies (Figure 8 (C)). From a comparison of the morphology/LIPSS distribution in Figure 8 (D) and (E) with the profiles of the etching pits (see Figure 3 (B)), it is noticeable that the smooth, HSFL-covered area in the center of the etch pits correlates roughly with the central zone I of the profile.

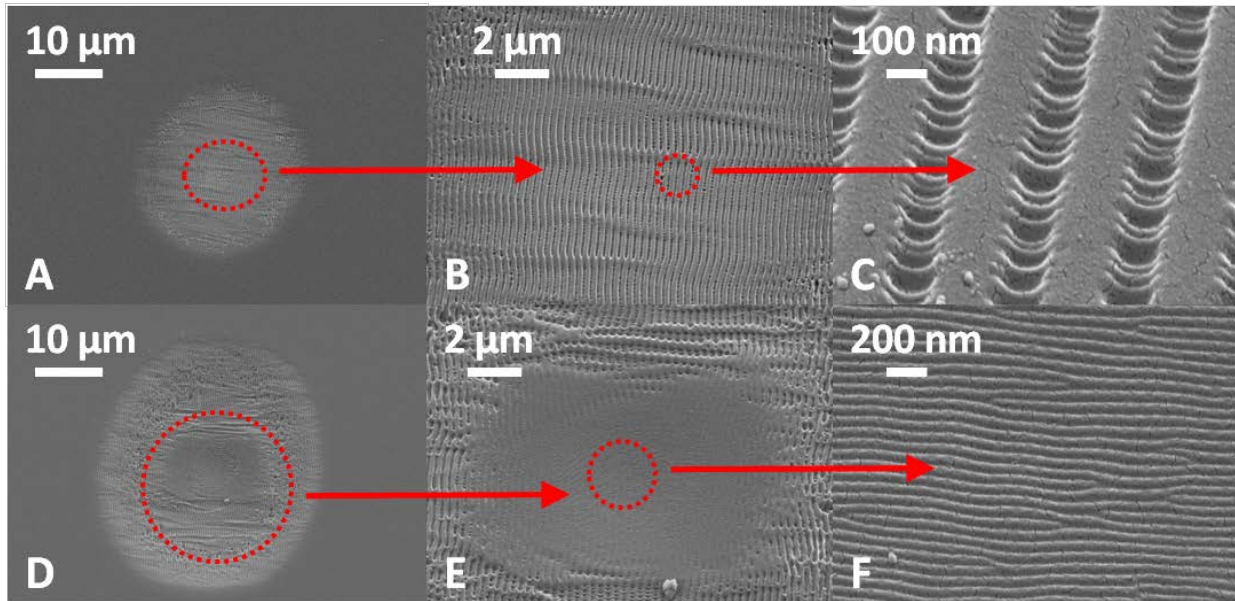


**Fig.8** SEM images of two etch pits at different magnifications after cleaning of the sample. The fluences for etching the pit in the upper (A to C) and lower (D to F) images were  $F = 5 \text{ J/cm}^2$  and  $F = 8 \text{ J/cm}^2$ , respectively. The period of the LSFL is  $\lambda_{\text{LSFL}} = 390 \pm 20 \text{ nm}$ , and the periods of the HSFL at low and high fluences (upper and lower rows) are  $\lambda_{\text{HSFL}} = 46 \pm 13 \text{ nm}$  and  $\lambda_{\text{HSFL}} = 52 \pm 2 \text{ nm}$ , respectively.

#### 4. Discussion

LIBWE processing of  $\text{SiO}_2$  with an aqueous  $\text{KMnO}_4$  solution as the absorber liquid by using laser pulses ( $\tau = 500 \text{ fs}$  and  $\lambda = 515 \text{ nm}$ ) was demonstrated. It was found that the etching rate increases with increasing fluence. By contrast, a reduction of the etching rate was found with larger pulse numbers  $N$ . In the etching pits, a layer of  $\text{MnO}_x$  could be found. After removal of the  $\text{MnO}_x$  layer by selective chemical etching, HSFL and LSFL can be observed in the etching pits.

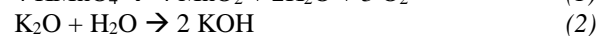
The achieved etching rate was very low in comparison to previously reported LIBWE experiments using nanosecond or ultrashort pulses [2, 16, 19, 35]. For example, in refs. [15-17], LIBWE experiments were reported with pyrene/toluene as the absorber liquid and with UV and NIR laser pulses that had pulse durations of  $\tau = 500 \text{ fs}$  and  $\tau = 150 \text{ fs}$ , respectively. In those studies [15-17], the observed etching rate was approximately one magnitude higher and the fluence range was about 10 times less than that in the present investigations. The division of the etching rate devolution into low- and high-fluence ranges is typical for the LIBWE process and has been observed with nanosecond laser pulses [32] and ultrashort laser pulses [19].

In the case of LIBWE with ultrashort laser pulses, these characteristics are discussed in relation to non-linear effects such as multi-photon absorption, which is more likely with higher laser energy densities.

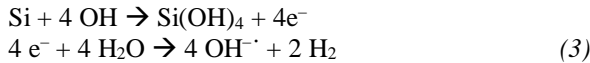
The observed decrease in the etching rate with an increase in the pulse number  $N$  for LIBWE with  $\text{KMnO}_4$  (see Figure 5) is the opposite of the characteristic reported for most other LIBWE experiments [3, 19, 36] with nanosecond or ultrashort laser pulses. A commonly reported

etch rate – pulse number dependency includes a specific number of laser pulses before etching starts (incubation), followed by a pulse number range, during which the etching rate increases, and a steady-state etching range, in which the etching rate is independent from the pulse number. For LIBWE with organic liquid absorbers, the required pulse number before etching starts and the increasing etching rate with an increase in the pulse number are explained with incubation effects [19, 36, 37]. In the LIBWE model given in ref. [1], a certain number of pulses is required to generate a thin defect-enriched surface layer, which can be ablated by the subsequent laser pulse and is reconstructed between the laser pulses. Hence, as a result of the extremely low etching rates, the extraordinary pulse number dependence, and the coverage of the etching pit with a rather thick  $\text{MnO}_x$  layer, the LIBWE model developed for hydrocarbon absorbers does not seem applicable. In consequence of this specific pulse number – etch rate dependency and the low achieved etching rate with the  $\text{KMnO}_4$  absorber, a specific etching mechanism is required for the non-hydrocarbon absorber.

Because the etching process with aqueous  $\text{KMnO}_4$  as the absorber liquid is affected by a variety of complex processes, a detailed description of the etching mechanism is difficult. Based on the experimental results, the following etching mechanism is proposed. The  $\text{KMnO}_4$  absorber liquid has a high absorption that was measured to be  $\alpha = 3.35 \mu\text{m}^{-1}$  at the laser wavelength of 515 nm [31]. Furthermore, thermal and photochemical decomposition can be assumed [38]; one dissociation pathway is given in Eq. 1. The formed  $\text{K}_2\text{O}$  can further react with water and form  $\text{KOH}$  in accordance with Eq. 2.



The aqueous KOH solution, which is known for etching SiO<sub>2</sub> [39], can dissolve silicon with the reaction scheme shown in Eq. 3 [40].



With standard KOH wet etching of SiO<sub>2</sub>, an etching rate of approximately 1 nm/s can be achieved, for example, by using a 30 % KOH solution at a temperature of  $T = 80 \text{ }^\circ\text{C}$  [41]. A comparison of the etching rates of the standard KOH wet etching with those of LIBWE using KMnO<sub>4</sub> is difficult. In contrast to the standard KOH wet etching, the temperature and concentration of the formed KOH can reach very high values locally at the surface for a short time; this can affect the etching process of SiO<sub>2</sub> by the decomposition of KMnO<sub>4</sub>.

The MnO<sub>x</sub> formed as a result of the photodissociation of KMnO<sub>4</sub> is deposited as a layer on the laser-processed area. With sufficient pulses, the thickness of the MnO<sub>x</sub> layer is high enough to prevent chemical etching of the SiO<sub>2</sub> by the KOH. As a result of the high optical absorption of MnO<sub>x</sub>, the thick MnO<sub>x</sub> layer provides an additional thin absorbing layer on the SiO<sub>2</sub> surface. Therefore, the laser energy is absorbed in the interface between the MnO<sub>x</sub> layer and the SiO<sub>2</sub> surface. The absorbed laser energy causes heating and partial or total ablation of the MnO<sub>x</sub> under confinement conditions and, in consequence, the formation of near-surface defects, such as structural deformation of the SiO<sub>2</sub>, attached impurities, or trapped electrons. The accumulation of these defects within the near-surface layer can enhance the absorption for subsequent laser pulses. With a sufficient density of defects and, therefore, free electrons, the laser energy can be absorbed by the free electrons and transferred via electron–phonon collision to the lattice (free-carrier model), which causes heating and evaporation of the SiO<sub>2</sub> lattice [17].

In addition, such structural defects are known to have an impact on the chemical etching of silicon dioxide [42]. The enhancement of chemical etching by KOH after femtosecond laser defect generation has been reported by Kiyama et al. [40]. The defects were generated by multiphoton processes directly in silica, which enabled selective etching of the irradiated regions provided with OH<sup>-</sup> ions. Because of the deposition of decomposition products from the KMnO<sub>4</sub> at the SiO<sub>2</sub> surface, the MnO<sub>x</sub> layer is regenerated after every laser pulse. In consequence, new absorbing layers at the SiO<sub>2</sub> surface are continually provided, which enables the deposition of the laser energy near the SiO<sub>2</sub> surface. Additionally to this suggested material removal process for high pulse numbers based on the generation of a defected enrich surface layer also mechanical ablation mechanisms have to be considered. Due to the different thermal expansion coefficients of the SiO<sub>2</sub> substrate and the adherent MnO<sub>x</sub> layer the substrate surface can be loaded with a high thermo - mechanical stress. This surface stress can supported or cause a material removal by e.g. “spallation”. A similar material removal process was described by G. A. Shafeev et al. [43] which investigated laser deposition of diamond – like films on transparent substrates from liquid hydrocarbons [44, 45].

The experimentally found dependencies of the etching rate and the MnO<sub>x</sub> layer thickness on the pulse number is supported by the proposed etching mechanism: For small pulse numbers and, in consequence, a thin MnO<sub>x</sub> layer, the high etching rate is dominated by chemical etching of the SiO<sub>2</sub> surface by the formed OH<sup>-</sup> ions. For high pulse numbers, the MnO<sub>x</sub> layer thickness increases and the etching rate decreases because of diffusion limitations. In this pulse number range, the material removal process is most likely dominated by the generation and ablation of a defect-enriched near-surface layer in the SiO<sub>2</sub> accompanied by thermo - mechanical surface stresses. Incubation processes could not be evaluated properly, because of the low absolute etching rate and the high pulse number needed for depth measurements. However, incubation might occur as a result of the defect-related wet etching process but could be superimposed with the formation of the OH<sup>-</sup> diffusion barrier, which results finally in a decrease of the etching rate with increasing pulse numbers. In general, the contribution of other processes to the process at low laser pulse range cannot be excluded. Apparently, no incubation has been found.

The low absolute value of the etching rate and the high fluence required for etching in comparison with LIBWE using an organic absorber could be caused by several factors, including the fact that, for the low pulse number range, the proposed dominant chemical etching process is less efficient than the defect-layer ablation-based process that occurs with LIBWE using an organic absorber. The dependency of the etching rate on the repetition rate (see Figure 5) could be explained with heat accumulation effects. As a result of heat accumulation at high repetition rates, thermal decomposition of KMnO<sub>4</sub> is quite likely, which assists in KOH etching of the SiO<sub>2</sub> surface. Furthermore, higher temperatures should enhance diffusion processes through the covering MnO<sub>x</sub> layer.

Inside the etching pit, two kinds of LIPSS can be found: HSFL and LSFL. The spatial period of the LSFL is  $\lambda_{\text{LSFL}} \approx 390 \pm 20 \text{ nm}$ . LSFL formations are commonly discussed with excitation of SPPs [25, 46]. Within the model of “perfect medium approximation” (PMA), one condition of excitation of SPP is given by Eq. 4 [47], in which  $\epsilon'$  is the real part  $Re(\epsilon)$  of the dielectric permittivity  $\epsilon$ .

$$\frac{\epsilon'_1 \epsilon'_2}{\epsilon'_1 + \epsilon'_2} > 0 \quad (4)$$

The spatial period of the SPP with the PMA model can be expressed by Eq. 5 [47].

$$\Lambda = \frac{\lambda}{\sqrt{\frac{\epsilon'_1 \epsilon'_2}{\epsilon'_1 + \epsilon'_2}}} \quad (5)$$

With consideration of the MnO<sub>x</sub> layer on the etched SiO<sub>2</sub> surface that can be seen in Figure 6 and the analysis of the MnO<sub>x</sub> layer thickness – pulse number dependency shown in Figure 7, it can be assumed that the SPP exist at the SiO<sub>2</sub>/MnO<sub>x</sub> interface. With  $\epsilon' = n^2 - k^2$  ( $n$  is the refraction index and  $k$  is the extinction coefficient),  $\epsilon' \approx 2.2$  for SiO<sub>2</sub> [48] and  $\epsilon' \approx 5.9$  for MnO<sub>2</sub> [49] at  $\lambda = 515 \text{ nm}$ . According to Eq. 4, excitation of SPP is possible at the

SiO<sub>2</sub>/MnO<sub>x</sub> interface. With Eq. 5, the calculated spatial period of the SPP is  $\Lambda = 407$  nm, which is close to the period of the LSFL ( $\lambda_{\text{LSFL}} \approx 390 \pm 20$  nm) that was found in the etching pits (see Figure 8). In contrast to the results of other studies [30], the LSFL are dominant for low fluences and the HSFL are dominant for high fluences. It is noticeable that the HSFL appear only in the central part of the etching pits, which feature two clearly distinguishable zones in the etching profile, as shown in Figure 3 (B). The period of the HSFL,  $\lambda_{\text{HSFL}} \approx (52 \pm 2)$  nm, is roughly equivalent to  $0.1 \times \lambda_{\text{Laser}}$ . This is much smaller than for reported HSFL in SiO<sub>2</sub>, for which the HSFL period was  $\lambda_{\text{HSFL}} \approx \lambda_{\text{Laser}}/4$  [50]. In several studies [30, 51], HSFL formation under water confinement was studied. It was shown that, because of water confinement, the period of the HSFL could be reduced up to a factor of five, relative to laser processing in air, depending on the sample material (e.g., Si:  $\lambda_{\text{HSFL,Air}} = 670$  nm,  $\lambda_{\text{HSFL,Water}} = 120$  nm [52]). The reason for the reduction in the periodicity is still under discussion. Proposed mechanisms for the periodicity reduction include effects such as inducing a non-linear refractive index [52] or plasmonic effects [30] as a result of the ultrashort laser pulses.

The observed characteristic that the LSFL are dominant for low fluences, whereas the HSFL are dominant for high fluences, which is the opposite to other studies [30], could be caused by the special interface conditions during LIBWE using KMnO<sub>4</sub> as an absorber liquid. The two distinguishable zones in the etching profile shown in Figure 3 (B) and the two areas of LIPSS show that the LIBWE conditions differ if low and high fluences are used. One possible reason for this characteristic could be found in the MnO<sub>x</sub> layer deposited in the etching pits. The MnO<sub>x</sub> layer can absorb, at high laser intensity, i.e., in the center of the Gaussian laser beam profile, sufficient energy to suffer partial removal during the laser irradiation by chemical or physical processes.

In the case of partial removal of the MnO<sub>x</sub> layer, the SiO<sub>2</sub> surface is in contact with the KMnO<sub>4</sub> solution, which results in a higher etching efficiency than that in the etching pit areas covered with the MnO<sub>x</sub> layer. These two different etching efficiencies in the laser irradiated area consequently cause the step in the etching profile shown in Figure 3 (B). Because of the partial removal of the MnO<sub>x</sub> layer, HSFL are generated at the interface between the SiO<sub>2</sub> surface and the aqueous KMnO<sub>4</sub> solution, which is an analogous condition to that for HSFL generation under water/SiO<sub>2</sub> confinement reported in [30, 51]. For the etched areas covered with the MnO<sub>x</sub> layer, LSFL are generated at the MnO<sub>x</sub>/SiO<sub>2</sub> interface, and the spatial period can be described by the PMA model (see Eq. 5).

## 5. Summary

LIBWE processing of SiO<sub>2</sub> by using KMnO<sub>4</sub> solution with 500 fs VIS laser pulses has been demonstrated for the first time. The observed etching rate is substantially less than that in other reported nanosecond or ultrashort pulse LIBWE experiments. The etching rate increases as the fluence increases. In contrast, the etching rate decreases with increases in the pulse number. In the laser-processed area, a

deposited MnO<sub>x</sub> layer can be found. A unique two-stage material removal mechanism has been proposed. For small pulse numbers, material removal is dominated by chemical etching of the SiO<sub>2</sub> surface by KOH, which is generated upon decomposition of KMnO<sub>4</sub>. For large pulse numbers, the main processes comprise laser-induced decomposition of KMnO<sub>4</sub>, deposition of a MnO<sub>x</sub> layer, defect formation near the surface of the SiO<sub>2</sub>, and selective laser ablation of the defect-enriched SiO<sub>2</sub>.

After cleaning of the samples, two kinds of LIPSS appear at the SiO<sub>2</sub> surface; these have been identified as LSFL and HSFL. LSFL with a period of  $\lambda_{\text{LSFL}} \approx 390 \pm 20$  nm are generated at low fluences at the edges of the LIBWE pits and can be explained by surface scattering of the laser light into SPP. Contrary to the usual experimental results, HSFL with a period of  $\lambda_{\text{HSFL}} \approx 52 \pm 2$  nm have been found in the center of the etching pit at high fluences after a large number of laser pulses. It can be concluded that HSFL are continually regenerated with this LIBWE process, because these are found at a depth of several hundreds of nanometers too. Hence, this experiment provides additional data to discuss the origin of HSFL formation.

## Acknowledgments

The authors would like to acknowledge Mr. Stolberg and Mrs. Hild (Jenoptik AG) for the possibility of the usage of the laser source for the experiments and the fruitful discussions. The authors would like to thank Dr. J. Bonse und Dr. J. Krüger (BAM) for helpful discussion about the LIPSS. This work was supported by the National Natural Science Foundation of China (NSFC) (No.11402120), the Natural Science Foundation of Jiangsu Province (Jiangsu Natural Science Foundation) (No. BK20140796), National Natural Science Foundation of China for International (Regional) Cooperation Research Project (No.11761131015), Fundamental Research Funds for the Central Universities (No.30918011345) and the Fundamental Research Funds for the Central Universities (No.30915015104).

## References

- [1] K. Zimmer, M. Ehrhardt, R. Boehme: *J. Appl. Phys.*, 107, (2010) 034908.
- [2] C. Vass, D. Sebok, B. Hopp: *Appl. Surf. Sci.*, 252, (2006) 4768.
- [3] X.M. Ding, T. Sato, Y. Kawaguchi, H. Niino: *Jpn. J. Appl. Phys.*, 42, (2003) 176.
- [4] H. Niino, Y. Kawaguchi, T. Sato, A. Narazaki, T. Gumpenberger, R. Kurosaki: *Appl. Surf. Sci.*, 252, (2006) 4387.
- [5] T. Sato, Y. Kawaguchi, R. Kurosaki, A. Narazaki, W. Watanabe, H. Niino: *J. Laser Micro Nanoengin.*, 6, (2011) 204.
- [6] K. Zimmer, R. Boehme, S. Pissadakis, L. Hartwig, G. Risse, B. Rauschenbach: *Appl. Surf. Sci.*, 253, (2006) 2796.
- [7] K. Zimmer, R. Boehme, D. Hirsch, B. Rauschenbach: *J. Phys. D*, 39, (2006) 4651.
- [8] J.-Y. Cheng, M.-H. Yen, T.-H. Young: *J. Micromech. Microeng.*, 16, (2006) 2420.

- [9] P. Lorenz, S. Zehnder, M. Ehrhardt, F. Frost, K. Zimmer, P. Schwaller: SPIE LASE, San Francisco, United States, (2014) p.89670A.
- [10] X.Z. Xie, M.F. Hu, W.F. Chen, X. Wei, W. Hu, X.Y. Gao, X.R. Yuan, M.H. Hong: *J. Laser Micro Nano Engin.*, 8, (2013) 259.
- [11] P. Schwaller, S. Zehnder, U. von Arx, B. Neuenchwander, Sixth International WLT Conference on Lasers in Manufacturing, Munich, Germany, (2011) p.188.
- [12] X. Xie, X. Huang, W. Jiang, X. Wei, W. Hu, Q. Ren: *Opt Laser Technol*, 89, (2017) 59.
- [13] S.I. Dolgaev, N.A. Kirichenko, G.A. Shafeev: *Appl. Surf. Sci.*, 138, (1999) 449.
- [14] S.I. Dolgaev, A.A. Lyalin, A.V. Simakin, G.A. Shafeev: *Appl. Surf. Sci.*, 96-8, (1996) 491.
- [15] R. Bohme, S. Pissadakis, M. Ehrhardt, D. Ruthe, K. Zimmer: *J. Phys. D*, 39, (2006) 1398.
- [16] R. Boehme, S. Pissadakis, M. Ehrhardt, T. Rudolph, D. Ruthe, K. Zimmer: 8th International Conference on Laser Ablation, Banff, Canada, (2007) p. 173.
- [17] R. Boehme, S. Pissadakis, D. Ruthe, K. Zimmer: *Appl. Phys. A*, 85, (2006) 75.
- [18] M. Ehrhardt, G. Raciukaitis, P. Gecys, K. Zimmer: *Appl. Phys. A*, 101, (2010) 399.
- [19] M. Ehrhardt, G. Raciukaitis, P. Gecys, K. Zimmer: *Appl. Surf. Sci.*, 256, (2010) 7222.
- [20] S. Zehnder, P. Lorenz, M. Ehrhardt, K. Zimmer, P. Schwaller: SPIE LASE, San Francisco, United States, (2014) p. 896812.
- [21] R. Boehme, C. Vass, B. Hopp, K. Zimmer: *Nanotechnology*, 19, (2008) 495301.
- [22] J. Bonse, M. Munz, H. Sturm: *J. Appl. Phys.*, 97, (2005) 013538.
- [23] A. Borowiec, H.K. Haugen: *Appl. Phys. Lett.*, 82, (2003) 4462.
- [24] D. Ashkenasi, A. Rosenfeld, H. Varel, M. Wähmer, E.E.B. Campbell: *Appl. Surf. Sci.*, 120, (1997) 65.
- [25] J. Bonse, S. Hoehm, S.V. Kirner, A. Rosenfeld, J. Krueger: *IEEE J. Sel. Top. Quantum Electron*, 23, (2017) 9000615.
- [26] X. Sedao, M.V. Shugaev, C. Wu, T. Douillard, C. Esnouf, C. Maurice, S. Reynaud, F. Pigeon, F. Garrelie, L.V. Zhigilei, J.P. Colombier: *ACS Nano*, 10, (2016) 6995.
- [27] X.F. Li, C.Y. Zhang, H. Li, Q.F. Dai, S. Lan, S.L. Tie: *Opt. Express*, 22, (2014) 28086.
- [28] S.N. Volkov, A.E. Kaplan, K. Miyazaki: *Appl. Phys. Lett.*, 94, (2009) 041104.
- [29] G.A. Martynovskii, G.D. Shandybina, D.S. Smirnov, S.V. Zaboltnov, L.A. Golovan, V.Y. Timoshenko, P.K. Kashkarov: *Opt. Spectrosc.*, 105, (2008) 67.
- [30] C. Albu, A. Dinescu, M. Filipescu, M. Ulmeanu, M. Zamfirescu: *Appl. Surf. Sci.*, 278, (2013) 347.
- [31] D.G. Lee, H. Karaman: *Can. J. Chem.*, 60, (1982) 2456.
- [32] R. Boehme, A. Braun, K. Zimmer: *Appl. Surf. Sci.*, 186, (2002) 276.
- [33] H. Niino, Y. Yasui, X.M. Ding, A. Narazaki, T. Sato, Y. Kawaguchi, A. Yabe: *J. Photochem. Photobiol.*, 158, (2003) 179.
- [34] S. Zehnder, P. Lorenz, M. Ehrhardt, K. Zimmer, P. Schwaller: SPIE, San Francisco, United States, (2014) 896812.
- [35] C. Vass, T. Smausz, B. Hopp: *J. Phys. D*, 37, (2004) 2449.
- [36] R. Bohme, K. Zimmer: *Appl. Surf. Sci.*, 247, (2005) 256.
- [37] M. Ehrhardt, P. Lorenz, P. Yunxiang, L. Bayer, B. Han, K. Zimmer: *Appl. Phys. A*, 123, (2017) 251.
- [38] F.H. Herbstein, M. Kapon, A. Weissman: *J. Therm. Anal. Calorim.*, 41, (1994) 303.
- [39] D.M. Knotter: "The Chemistry of Wet Etching". In: "Handbook of Cleaning in Semiconductor Manufacturing", (John Wiley & Sons Inc., New York, 2011) pp. 95.
- [40] S. Kiyama, S. Matsuo, S. Hashimoto, Y. Morihira: *J. Phys. Chem. C*, 113, (2009) 11560.
- [41] H. Seidel, L. Csepregi, A. Heuberger, H. Baumgörtel: *J. Electrochem. Soc.*, 137, (1990) 3612.
- [42] T. Tetsuya, F. Seiichi, K. Shingo: *J. Appl. Phys.*, 32, (1993) 6114.
- [43] A.V. Simakin, E.N. Lubnin, G.A. Shafeev: *Quantum Electron*, 30, (2000) 263–267. [44] A.A. Lyalin, A.V. Simakin, V.A. Bobyrev, E.N. Lubnin, G.A. Shafeev: *Quantum Electron*, 29, (1999), 355.
- [45] A.A. Lyalin, A.V. Simakin, Loubnin, G.A. Shafeev: *Thin Solid Films*, 357, (1999) 144.
- [46] F. Garrelie, J.P. Colombier, F. Pigeon, S. Tonchev, N. Faure, M. Bounhalli, S. Reynaud, O. Parriaux: *Opt. Express*, 19, (2011) 9035.
- [47] J.Y.D. Thibault, K. Jörg, B. Jörn: *J. Opt.*, 18, (2016) 115007.
- [48] L. Gao, R. Lemarchand, M. Lequime: *J. Eur. Opt. Soc. Rapid Publ.*, 8, (2013) 13010.
- [49] S.K. Hazaa: *Berkala Fisika Indonesia*, 5, (2013) 01.
- [50] R. Wagner, J. Gottmann, 8th International Conference on Laser Ablation, Banff, Canada, (2007), p.333.
- [51] T.J.Y. Derrien, R. Koter, J. Krueger, S. Hoehm, A. Rosenfeld, J. Bonse: *J. Appl. Phys.*, 116, (2014) 074902.
- [52] C. Wang, H. Huo, M. Johnson, M. Shen, E. Mazur: *Nanotechnology*, 21, (2010) 075304.

(Received: December 19, 2017, Accepted: May 10, 2018)